Upconversion Emission Enhancement in Yb3+/Er3+–Codoped Y2O3 Nanocrystals by Tridoping with Li+ Ions

5 AUTHORS, INCLUDING:

Guanying Chen
Harbin Institute of Technology
70 PUBLICATIONS **2,549** CITATIONS

SEE PROFILE

Haichun Liu
Lund University
26 PUBLICATIONS **384** CITATIONS

SEE PROFILE

Zhiguo Zhang
131 PUBLICATIONS **1,568** CITATIONS

SEE PROFILE

Upconversion Emission Enhancement in Yb³⁺/Er³⁺-Codoped Y₂O₃ Nanocrystals by Tridoping with Li⁺ Ions

Guanying Chen, Haichun Liu, Huijuan Liang, Gabriel Somesfalean, and Zhiguo Zhang*

Department of Physics, Harbin Institute of Technology, 150001 Harbin, People's Republic of China

Received: May 8, 2008

We demonstrate that tridoping with Li⁺ ions enhances the visible green and red upconversion (UC) emissions in Er³⁺/Yb³⁺-codoped Y₂O₃ nanocrystals by up to half of the bulk counterpart, i.e., about 2 orders of magnitude higher than previous results. X-ray diffraction and decay time investigations give evidence that tridoping with Li⁺ ions can tailor the local crystal field of the Y₂O₃ host lattice. Theoretical calculations illustrate well that a significant UC intensity enhancement arises from the synthesized tailoring effect induced by the Li⁺ ions, which increase lifetimes in the intermediate ⁴I₁₁/₂ (Er) and ²F₅/₂ (Yb) states, increase optically active sites in the Y₂O₃ host lattice, and dissociate the Yb³⁺ and Er³⁺ ion clusters in the nanocrytals. The general theoretical description of the visible UC radiations shows that the Yb³⁺ ion sensitization and the tailoring effect induced by the Li⁺ ions are two independent enhancement mechanisms, which is expected to lead to an increasing number of photonic and biomedical applications in the future.

Introduction

Inorganic nanocrystals doped with trivalent rare-earth ions can easily up-convert the absorbed near-infrared (NIR) light into visible light by use of cost-effective and high-power NIR diode lasers.[1,2] This is due to the fact that rare-earth ions usually have an energy level structure of equally spaced long-lived excited states.[3] Inorganic UC phosphors have found a number of potential applications such as nanoceramics for volumetric displays,[4] temperature sensors,[5] UC lasers,[6] biomedical imaging,[7,8] DNA detection,[9] and photodynamic therapy.[10] Insufficient intensity, however, still constitutes the main limitation for practical applications of nanosized UC materials.[1,2,11] Among inorganic nanocrystals, oxides exhibit higher mechanical, thermal, and chemical stability and constitute a challenging candidate for biomedical and photonic applications.[4–8] Realization of efficient NIR to visible UC in oxide nanocrytals will have great impact in deploying their potential advantages.

Yttrium oxide (Y₂O₃) doped with Er³⁺ ions sensitized by Yb³⁺ ions has been established as one of the model UC systems for generating efficient visible radiation under laser excitation of 970 nm.[3,12–17] This is not only because Y₂O₃ has high chemical and mechanical durability, high thermal stability, excellent optical properties, and relatively low phonon cutoff energy, but also because the Er³⁺ ion has a favorable energy level structure that matches the 970 nm pump laser, which is in good agreement with the large absorption peak of Yb³⁺ ions.[16] Experimental investigations evidenced that the Yb³⁺/Er³⁺-codoped Y₂O₃ nanocrytals can emit UC radiations that are about 1 or 2 orders of magnitude higher than the solely Er³⁺-doped Y₂O₃ nanocrystals (depending on the Yb³⁺ concentration), because the Yb³⁺/Er³⁺-codoped materials utilize the sensitizing mechanism to produce UC luminescence, in marked contrast to that of single Er³⁺-doped materials.[3,15,17] The high UC radiation achieved has garnered considerable attentions in the literature but, unfortunately, still falls short for many practical applications. It is, therefore, of great interest to further signifi-

cantly increase the UC radiations in the Yb³⁺/Er³⁺-codoped Y₂O₃ nanocrystals.

As for the UC enhancement, Gouveia-Neto et al. have reported 3-fold UC enhancement in chalcogenide glass by thermally increasing the phonon-assisted side absorption of the Yb³⁺ ions at a nonresonant excitation of 1.064 μm.[18] Additionally, they have fabricated transparent glass vitroceramics to gain higher UC radiation than in the glass matrix by concentrating rare-earth ions into precipitated PbF₂ nanocrytals that have much lower phonon energy.[19] Chow et al. have gained about 1 order of magnitude enhancement for the Yb³⁺/Er³⁺-codoped NaYF₄ nanocrystals by growing a NaYF₄ shell on them, thereby eliminating the drawbacks from surface contaminants of high phonon energy, defects in the host lattice, and large fraction of surface-bond rare-earth ions.[20] A similar core/shell strategy was also used to enhance the UC radiations by about 4 times in Er³⁺-doped ZrO₂ nanocrytals, which, however, was interpreted as compensating a ligand crystal field of silica shell on the surface Er³⁺ ions.[21] However, material engineering of the local crystal field around the rare-earth ions in the host lattice to increase their UC radiations by orders of magnitude has rarely been reported, except for in our recent work[22] and in ref 23 on UC enhancement in Er³⁺-doped Y₂O₃ nanocrystals.

Generally speaking, the main intra-4f electronic-dipole transitions of rare-earth ions are forbidden by the quantum mechanical selection rules, which, however, can be broken by the local crystal field of the rare-earth ions due to the capability to intermix their f states with higher electronic configurations.[1,24] Consequently, tailoring the local crystal field of the rare-earth ions and thereby the radiation parameters might become an alternative general strategy to increase the UC emissions for various host materials doped with diverse rare-earth ions. The Li⁺ ion has the smallest cationic radius in the periodical table of elements, which is favorable for their movement and site occupation in the host lattice. These advantages make them attractive for use in tailoring of the host lattice local crystal field.

Here we report on a 25 times enhancement of the visible UC radiation in Y₂O₃/Yb³⁺/Er³⁺ nanocrystals by tridoping with Li⁺

ions. The systematic experimental investigations of Li⁺ ions' effect on the radiation lifetimes of intermediate $^4I_{11/2}$ (Er) and $^2F_{5/2}$ (Yb) states and on the UC enhancement increase are presented. Theoretical calculations have been used to interpret the observed enhancement increase for the visible UC radiations by means of the measured radiation lifetimes and the intensity ratio of the green-to-red UC. It is found that the high UC radiations achieved in Y_2O_3/Yb³⁺/Er³⁺/Li⁺ nanocrystals gain simultaneously from two independent enhancement mechanisms, including the sensitizing merits of the Yb³⁺ ions as well as the tailoring merits of the Li⁺ ions. Additionally, the dependence of the UC enhancement in bulk ceramic Y_2O_3 by Li⁺ ion doping is also experimentally investigated and briefly discussed.

Experimental Section

1. Sample Preparation. The ion concentration of 2 mol % of Yb³⁺ was selected for codoping in Y_2O_3/Er³⁺ 1 mol % nanocrystals, since the green and red UC radiations thereby obtained have similar intensities, which facilitates the enhancement analysis. The synthesis of Y_2O_3 doped with 1 mol % of Er³⁺, 2 mol % of Yb³⁺, and 0, 2, 5, 7, 10, or 15 mol % of Li⁺ ions, were adapted from a previously published procedure:[8] yttrium nitrate (99.99%), erbium nitrate (99.99%), ytterbium nitrate (99.99%), and lithium nitrate (99.99%) with corresponding mole ratios, were first completely dissolved in deionized water. Subsequently, citric acid was added into the solution with a mole ratio of (Y + Er + Yb + Li) to citric acid of 1:4. After complete dissolution, the pH of the solution was adjusted to 6.0 by the addition of ammonium hydroxide. The resulting solution was dried at 120 °C for 24 h until it was transformed into a black bulk, which was further calcined at 800 °C for 2 h in air. The bulk ceramic Y_2O_3 doped with 1 mol % of Er³⁺ and 2 mol % of Yb³⁺ ions, and the bulk ceramic Y_2O_3 further tridoped with 5 mol % of Li⁺ ions, were obtained by sintering the corresponding pressed nanopowder disks (Y_2O_3 nanocrystals doped with 1 mol % of Er³⁺ and 2 mol % of Yb³⁺ ions, and Y_2O_3 nanocrytals further tridoped with 5 mol % of Li⁺ ions, respectively) in a tubular furnace at 1300 °C for 24 h in air.

2. Characterization. The powder X-ray diffraction (XRD) patterns were recorded by a Rigaku D/max-γB diffractometer using Cu Kα radiation ($\lambda = 0.15418$ nm). The 2θ angle of the XRD spectra was recorded at a scanning rate of 5 °/min. The average crystallite sizes of the nanocrystals were calculated according to Scherrer's equation,[25]

$$D = K\lambda/(\beta \cos \theta) \qquad (1)$$

where $K = 0.89$, D represents the crystallite size (in nanometers), λ is the wavelength of the Cu Kα radiation, β is the corrected half-width of the diffraction peak, and θ is Bragg's angle of the diffraction peak. Fourier transform infrared (FT-IR) spectra were measured with a BRUKER IFS 66v/S infrared spectrometer via the potassium bromide (KBr) pellet technique. In making the KBr pelletes, 1 mg of sample was diluted with approximately 100 mg of KBr powder. Each FT-IR spectrum was collected in the spectral range of 400–4000 cm⁻¹.

3. Measurements. The as-prepared powders were pressed to form smooth and flat disks to be utilized for spectral studies by irradiation with a focused 500 mW power-controllable 970 nm diode laser (Hi-Tech Optoelectronics Co. Ltd., Beijing). The focus area on the disk sample was measured to be about 1 mm². The emitted UC fluorescence was collected by a lens-coupled monochromator (Zolix Instruments Co. Ltd., Beijing) of 3 nm spectral resolution with an attached photomultiplier tube (Hamamatsu CR131). All spectral measurements were per-
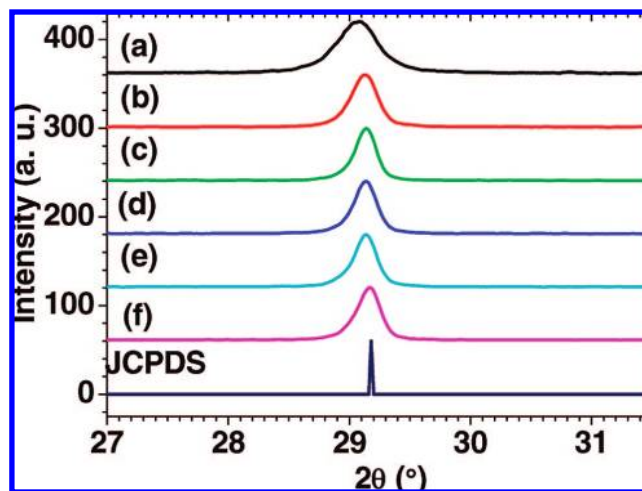

Figure 1. Measured XRD spectra of Y_2O_3 powders doped with 1 mol % of Er³⁺, 2 mol % of Yb³⁺ ions, and further tridoped with Li⁺ ion concentrations of (a–e) 0, 2, 5, 7, 10, and 15 mol %, contrasted with (f) the standard pattern of JCPDS 05 0574.

formed at room temperature, preserving the same geometry for the UC luminescence recording. Decay profiles of the 1015 and 1075 nm radiations were measured by square-wave-modulation of the electric current input to the 970 nm diode laser and by recording the signals via a Tektronix TDS 5052 digital oscilloscope with a lock-in preamplifier (Stanford Research System Model SR830 DSP) employing a chopping rate of 3000 rps. The photomultiplier tube was replaced by a NIR-sensitive InGaAs photodiode (Thorlabs, DET 410/M) when measuring the decay profiles and the fluorescence spectra of the light in the NIR range.

Results

1. Structure and Nanocrystal Size. Figure 1 shows the XRD patterns of the Y_2O_3 powders doped with 1 mol % of Er³⁺, 2 mol % of Yb³⁺ ions, and tridoped with 0–15 mol % of Li⁺ ions. The main diffraction peaks are exclusively displayed in order to clearly present their positions and widths. As shown in the figure, all powders are of cubic structure, corresponding well to the standard pattern of Y_2O_3 (JCPDS 05 0574) referenced below. The main diffraction peak shifts toward larger angles for Li⁺ ion concentrations of 0–2 mol %, then gradually moves reversely for Li⁺ ion concentrations of 2–7 mol %, and finally remains almost constant for Li⁺ ion concentrations higher than 7 mol %. Substituting the Y³⁺ ion by the smaller Li⁺ ion can cause the host lattice to shrink, whereas occupying the interstitial sites can cause the host lattice to expand. Consequently, the peak shifting result indicates that the effect on the cell parameters induced by Y³⁺-site substitution dominates over that of interstitial site occupation for Li⁺ ion concentrations of 0–2 mol % and reverses for Li⁺ ion concentrations of 2–7 mol %. The constant peak position for Li⁺ ion concentrations above 7 mol % suggest that no further Li⁺ ions can enter into the Y_2O_3 host lattice, which can further be demonstrated by the same decay profiles of Yb³⁺ and Er³⁺ ions in these samples (see Figure 8). It should be noted that both the substitution of Y³⁺ ions and the occupation of interstitial sites can tailor the local crystal field around the Er³⁺ ions in the host lattice, which expectedly affects their UC luminescence. According to eq 1, the average sizes of the Y_2O_3 nanocrystals doped with 1 mol % of Er³⁺, 2 mol % of Yb³⁺ ions, and tridoped with Li⁺ ion concentrations of 0, 2, 5, 7, 10, and 15 mol %, are calculated
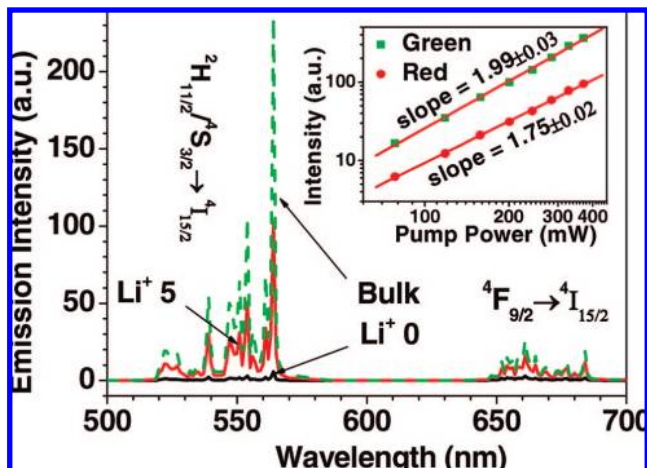
Figure 2. Measured UC spectra of nanocrystals and bulk Y_2O_3 doped with 1 mol % of Er^{3+} and 2 mol % of Yb^{3+} ions and Y_2O_3 nanocrystals further tridoped with 5 mol % of Li^+ ions under laser excitation of 970 nm. The inset is the pump power dependence of the green and red UC emissions in Y_2O_3 nanocrystals tridoped with 5 mol % of Li^+ ions.

to be about 44, 54, 58, 58, 58, and 54 nm, respectively. This indicates that the Y_2O_3 nanocrystals grow slightly with the introduction of Li^+ ions but without further increase at higher Li^+ ions.

2. Contrasted UC Luminescence. Figure 2 shows the UC radiation in untailored Y_2O_3 nanocrystals doped with 1 mol % of Er^{3+} and 2 mol % of Yb^{3+} ions; tailored Y_2O_3 nanocrystals doped with 1 mol % of Er^{3+}, 2 mol % of Yb^{3+}, and 5 mol % of Li^+ ions; and bulk Y_2O_3 doped with 1 mol % of Er^{3+} and 2 mol % of Yb^{3+} ions, respectively, under 970 nm diode laser excitation of about 40 W/cm². The inset presents the pump power dependence of the green and red UC emissions in Y_2O_3 nanocrystals doped with 1 mol % of Er^{3+}, 2 mol % of Yb^{3+} ions, and tridoped with 5 mol % of Li^+ ions. As illustrated in Figure 2, the green and red UC bands centered at 560 and 650 nm arise from the intra-4f electronic transitions $^2H_{11/2}/^4S_{3/2} \rightarrow$ $^4I_{15/2}$ and $^4F_{9/2} \rightarrow {}^4I_{15/2}$ of the Er^{3+} ions, respectively.[3] Generally, these UC radiations in inorganic nanocrystals without particular treatment present UC radiations about 2 orders of magnitude lower than that of their bulk counterpart, for example, the most efficient nanocrystals $NaYF_4$; 20 mol % of Yb^{3+} and 2 mol % of Er^{3+} is about $10^2\sim10^3$ less efficient than their bulk counterpart.[26] Similar phenomena were also observed here (see Figure 2), where the bulk ceramic Y_2O_3 doped with 1 mol % of Er^{3+} and 2 mol % of Yb^{3+} ions presents UC emissions about 50 times higher than the untailored Y_2O_3 nanocrystals doped with 1 mol % of Er^{3+} and 2 mol % of Yb^{3+} ions. Interestingly, the fluorescent UC radiations in Li^+-ions tailored Y_2O_3 nanocrystals (doped with 1 mol % of Er^{3+}, 2 mol % of Yb^{3+}, and 5 mol % of Li^+ ions) were enhanced up to about half of the corresponding bulk ceramic Y_2O_3 without Li^+ ions. This result clearly indicates that the enhancement strategy via Li^+ ion doping allows the UC nanocrystals to radiate like the bulk counterpart, which obviously can promote their potential applications in photonics and biomedicine, such as for temperature sensors and biolabeling. It should be noted that for biolabeling, synthesizing monodisperse Y_2O_3 nanocrytals of less than 10 nm with proper surface modification will be required, which, however, will not degrade the effectiveness of the Li^+ ion doping for inducing the significant UC radiation increase in these nanocrystals. This is because engineering of the local crystal field of the Y_2O_3
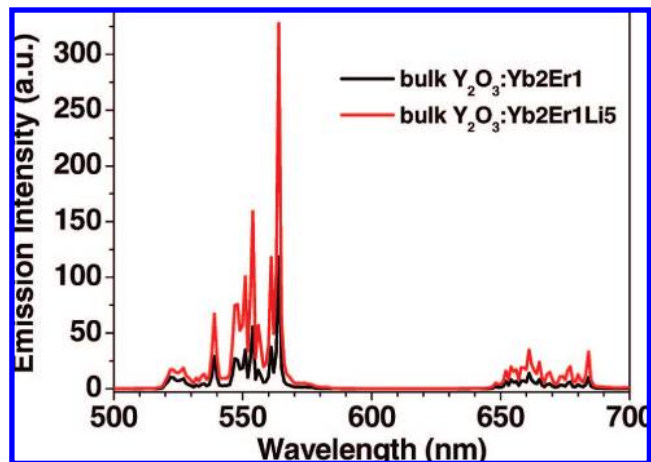

Figure 3. Measured UC emissions of ceramic bulk Y_2O_3 doped with 2 mol % of Yb^{3+} and 1 mol % of Er^{3+} ions and further tridoped with Li^+ ion concentrations of 0 and 5 mol %, respectively.
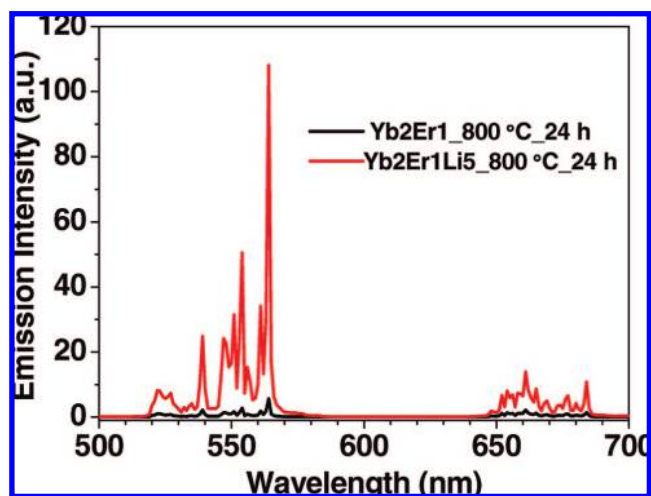

Figure 4. Measured UC emissions of Y_2O_3 powders that were sintered at 800 °C for 24 h, doped with 2 mol % of Yb^{3+} and 1 mol % of Er^{3+} ions and further tridoped with Li^+ ion concentrations of 0 and 5 mol %, respectively.

host lattice constitutes the enhancement strategy without considering shape and size.

Figure 3 presents the UC emission of ceramic bulk Y_2O_3 doped with 2 mol % of Yb^{3+} and 1 mol % of Er^{3+} and further tridoped with Li^+ ion concentrations of 0 and 5 mol %, respectively. As shown in the figure, the tridoping with Li^+ ions can also lead to a remarkable increase in ceramic bulk Y_2O_3 (by about 3 times), which suggests the effectiveness of Li^+ ion-doping for the UC enhancement in bulk crystals. It is worthwhile to mention that smaller intensity enhancement was observed in ceramic bulk than in nanocrystals, which arises from the fact that some of the Li^+ ions can escape from the Y_2O_3 host lattice when sintering at a high temperature of 1300 °C for 24 h. Such a conclusion can be verified by reducing the sintering temperature. Figure 4 displays the UC emissions of Y_2O_3 powders doped with 2 mol % of Yb^{3+} and 1 mol % of Er^{3+} ions and tridoped with Li^+ ion concentrations of 0 and 5 mol %, respectively, achieved by sintering the corresponding nanocrytaldisks in a tubular furnace at 800 °C for 24 h. As shown in Figure 4, similar enhancement results were observed as expected for Y_2O_3 nanocrystals. To improve the performance of the (transparent) ceramic bulk, which is best made of oxide nanocrystals for use in nanoceramics for volumetric displays or UC lasers,[4,6]
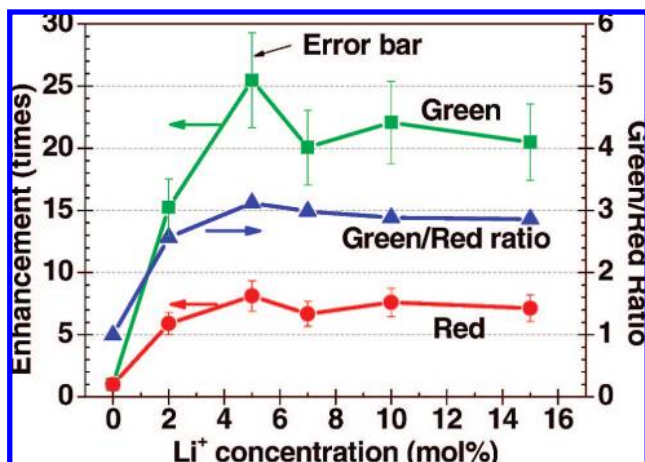
Figure 5. Enhancement times of the green and red UC as well as the green-to-red intensity ratio in Y_2O_3 nanocrystals as a function of Li^+ ions under laser excitation of 970 nm.

appropriate annealing techniques will be needed to realize the large Li^+ ion doping into the ceramic for higher UC enhancement.

3. Enhancement of the UC Luminescence. Figure 5 illustrates the enhancement of the green and red UC emissions as well as the green-to-red intensity ratio in Y_2O_3 nanocrystals doped with 1 mol % of Er^{3+}, 2 mol % of Yb^{3+} ions, and with various Li^+ ions under 970 nm diode laser excitation of 40 W/cm². It should be noted that different scales were used as marked by arrows in the figure. As shown in Figure 5, the green and red UC emissions both increase dramatically with Li^+ ion concentrations of 0−5 mol % and remain almost constant at higher Li^+ ions. The maximum UC green and red enhancement, for the suboptimal experimental conditions presented here, are about 25 times and 8 times greater, respectively, corresponding to Li^+ ion concentrations of 5 mol %. As for the intensity ratio, it increases about three times for Li^+ ion concentrations of 0−5 mol % and remains nearly constant at higher Li^+ ion concentrations. It is expected that for the constant Er^{3+} and Yb^{3+} ion-doping present here there should be an equally constant intensity ratio of the green-to-red for all the Li^+ ion concentrations. The increased intensity ratio at low Li^+ ions indicates that the cross relaxation (CR) and the energy back transfer (EBT) processes involved in the red UC generation are hindered by the dissociation of both the Er^{3+} and the Yb^{3+} clusters via tridoping with Li^+ ions (see Figure 8).[22] Such a mechanism can also explain the green and red UC enhancement discrepancy in Figure 5.

Discussions

1. Nonradiative Process Analysis. The UC efficiency is principally governed by nonradiative processes in materials,[27] which are dependent on the energy gap separating the upper and lower levels as well as the highest phonon energy in the materials.[28] The multiphoton nonradiative decay rate can be expressed as eq 2,[27]

$$W_n(T) = W_0(0)[1 - \exp(-h\nu/kT)]^{-n} \qquad (2)$$

where $W_n(T)$ is the rate at temperature T, $W_0(0)$ is the rate at 0 K, $n = \Delta E/h\nu$, $h\nu$ is the relevant phonon cutoff energy, and ΔE is the energy gap involved. According to this equation, the lower phonon cutoff energy can increase the UC emission by hindering nonradiative relaxations, for example, the fluoride and chloride materials are more UC luminescent than the oxide materials due to the lower phonon cutoff energy.
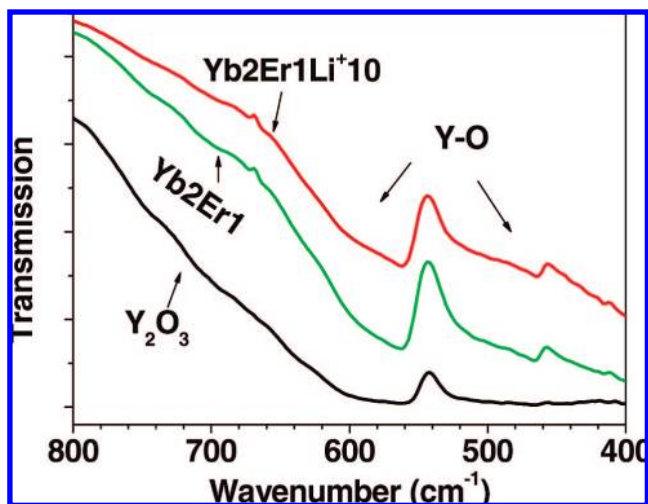

Figure 6. Measured FT-IR transmission spectra of commercial Y_2O_3 powders as well as of prepared Y_2O_3 nanocrystals doped with 1 mol % of Er^{3+}, 2 mol % of Yb^{3+} ions, and further tridoped with a Li^+ ion concentration of 10 mol %.
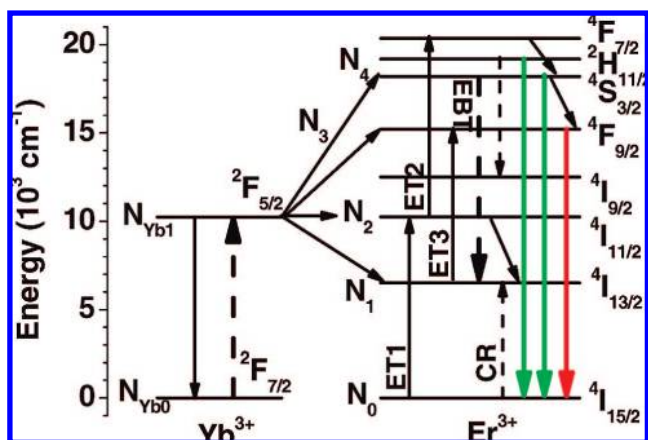

Figure 7. Energy level diagrams of the Er^{3+} and Yb^{3+} ions as well as the proposed UC mechanisms for the green and red emissions.

Figure 6 presents the FT-IR transmission spectra of commercial Y_2O_3 powders, Y_2O_3 nanocrystals doped with 2 mol % of Yb^{3+} and 1 mol % of Er^{3+} ions, and Y_2O_3 nanocrystals further doped with a Li^+ ion concentration of 10 mol %, respectively. The absorption bands at 570 and 450 cm⁻¹ arise from the vibration mode of Y−O, which agree well with the reported phonon cutoff energy.[24] As illustrated in Figure 6, the phonon cutoff bands at 570 cm⁻¹ are almost identical for the three samples, which indicates that the lattice vibration mode, and thereby the multiphonon nonradiative rate, has not been changed by further doping with Li^+ ions. It is worthwhile to point out that the absorption bands of the surface contaminants (OH and CO groups) were measured to be about the same for Y_2O_3 nanocrystals doped without and with various Li^+ ions (see Supporting Information).[28] Therefore, their effect on the UC efficiency, if any, should be about the same for all the prepared powders doped with various Li^+ ions.

2. General Theoretical Descriptions for UC Green and Red Luminescence. Figure 7 presents the energy level diagrams of the Yb^{3+} and Er^{3+} ions and the proposed mechanism to produce visible fluorescent radiation. As illustrated in Figure 7, two energy transfers (ET 1 and 2) from Yb^{3+} ions can promote the Er^{3+} ion to the $^4F_{7/2}$ state. The efficient EBT $^4S_{3/2}$ (Er) + $^2F_{7/2}$(Yb) → $^4I_{13/2}$ (Er) + $^2F_{5/2}$ (Yb) and the CR $^2H_{11/2}$ (Er) + $^4I_{15/2}$ (Er) → $^4I_{9/2}$ (Er) + $^4I_{13/2}$ (Er) processes can populate
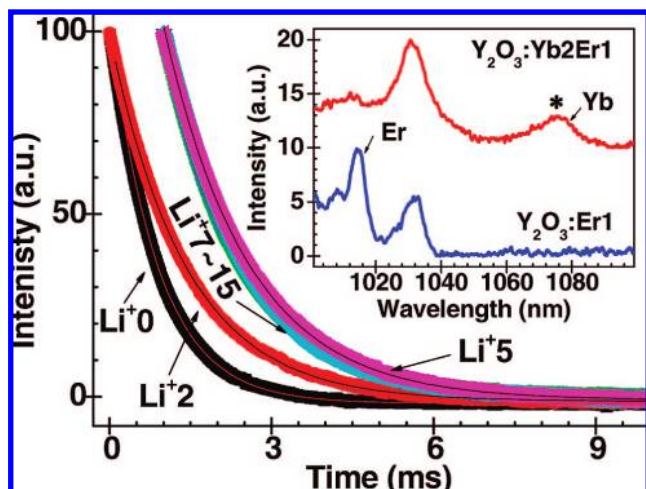
Figure 8. Decay profiles of the $^2F_{5/2}$ (Yb) → $^2F_{7/2}$ (Yb) transition in Y$_2$O$_3$ nanocrystals tridoped with 0, 2, 5, 7, 10, 15 mol % of Li$^+$ ions. The inset presents the contrasted fluorescence spectrum in Y$_2$O$_3$/1 mol % of Er^{3+} and Y$_2$O$_3$/1 mol % of Er^{3+} and 2 mol % of Yb^{3+} nanocrystals under laser excitation of 970 nm.

the $^4I_{13/2}$ (Er) state, which is further excited to the $^4F_{9/2}$ (Er) state (by use of ET 3) for the red UC emission.[12–15,25] In marked contrast to single Er^{3+}-doped materials, the ground-state and the excited-state absorptions of Er^{3+} ions are neglected here, since the Yb^{3+} ions have a much larger absorption cross section and efficiently transfer energy to the Er^{3+} ions.[2]

To make a general theoretical description for the green and red UC emissions, we utilized the following steady-state equations:

$$\frac{dN_1}{dt} = 0 = W'N_4N_{Yb0} + CN_4N_0 - W_1N_{Yb1}N_1 - N_1/\tau_1 \tag{3.1}$$

$$\frac{dN_2}{dt} = 0 = W_0N_{Yb1}N_0 - W_2N_{Yb1}N_2 - N_2/\tau_2 \tag{3.2}$$

$$\frac{dN_3}{dt} = 0 = W_1N_{Yb1}N_1 + W_{non}N_4 - N_3/\tau_3 \tag{3.3}$$

$$\frac{dN_4}{dt} = 0 = W_2N_{Yb1}N_2 - N_4/\tau_4 \tag{3.4}$$

$$\frac{dN_{Yb1}}{dt} = 0 = \rho\sigma_{Yb}N_{Yb0} + W'N_4N_{Yb0} - (W_0N_0 + W_1N_1 +$$
$$W_2N_2)N_{Yb1} - N_{Yb1}/\tau_{Yb} \tag{3.5}$$

$$N = N_0 + N_1 + N_2 + N_3 \approx N_0 \tag{3.6}$$

$$1/\tau_4 = 1/\tau_{rad} + W_{non} + CN_0 + W'N_{Yb0} \tag{3.7}$$

$$\beta_{green} \equiv \tau_4/\tau_{rad} \tag{3.8}$$

where $N_0(W_0)$, N_1 (W_1, τ_1), N_2 (W_2, τ_2), N_3 (τ_3), and N_4 (τ_4) are the population densities (energy transfer rates from excited Yb^{3+} ions, decay time) of the $^4I_{15/2}$, $^4I_{13/2}$, $^4I_{11/2}$, $^4F_{9/2}$, and $^4S_{3/2}$ states of the Er^{3+} ions, respectively; N_{Yb0} and N_{Yb1} are the population densities of Yb^{3+} ions in the ground and the excited states, respectively; W' is the EBT rate to the Yb^{3+} ion; ρ is the laser photon number density; σ_{Yb} denotes the absorption cross section of the Yb^{3+} ion; τ_{rad} is the radiation lifetime of the $^4S_{3/2}$ state; and W_{non} is the nonradiative decay rate of the $^4S_{3/2}$ state to the $^4F_{9/2}$ state. The $W'N_4N_{Yb0}$ in eq 3.5 is neglected in the following discussions since its contribution to N_{Yb1} is much lower than

that induced by laser population.[25] Additionally, the UC or ET rates in the $^4I_{11/2}$ (Er) and $^2F_{5/2}$ (Yb) states are supposed to be much lower than their decay rates,[14,29] which reverses for the $^4I_{13/2}$ (Er) state due to its longest lifetime.[25] According to eqs 3.1–3.8, we can easily derive a general theoretical description of the fluorescent radiations.

$$I_{green} = N_4/\tau_{rad} = \beta_{green}\tau_{Yb}^2\tau_2(\sigma_{Yb}N_{Yb0})^2\rho^2(W_2W_0N_0) \propto \rho2 \tag{4}$$

$$I_{red} = (1/\beta_{green} - 1)I_{green} \tag{5}$$

Equations 4 and 5 show that the green and red UC radiations will have a quadratic power dependence on the laser power, which agrees well with the observations in the inset of Figure 2. Such an agreement suggests the correctness of the theoretical aproach. As illustrated in eq 4, the green UC fluorescent intensity strongly depends on the luminescent population ratio in the $^4S_{3/2}$ state (β_{green}), the lifetimes of the intermediate $^2F_{5/2}$ (Yb) and $^4I_{11/2}$ (Er) states ($\tau_{Yb}^2\tau_2$), the absorption cross section and the concentration of Yb^{3+} ions [$(\sigma_{Yb}N_{Yb0})^2$], the laser pump power density (ρ^2), the Er^{3+} concentration (N_0), and the energy transfer coefficients of ET 1 and 2 (W_2W_0). It should be noted that the same pump power density was utilized for the comparison of UC emissions, which means a constant parameter ρ^2 for all Y$_2$O$_3$ nanocrystals. Furthermore, the same ion concentrations of 1 mol % of Er^{3+} and 2 mol % of Yb^{3+} are employed for all nanocrystals, which may suggest the same $(\sigma_{Yb}N_{Yb0})^2$, N_0, and W_2W_0 parameters for all the samples. The question is if that would also be true for the concentration parameters N_0 and N_{Yb0}? It is noted that trivalent Er^{3+} and Yb^{3+} ions can enter the Y$_2$O$_3$ lattice by isomorphic substitution of Y^{3+} without charge compensation. There are two different types of substitutional sites in the unit cell: three of point-group symmetry C_2 and one of point-group symmetry C_{3i}. Because the C_{3i} sites have inverse symmetry, the main electric-dipole transitions are forbidden for the rare earth ions at this site.[24] However, such banned transitions can become allowed for Li$^+$ ion-tailored nanocrytals, since the inversion symmetry can be easily destroyed by the interstitial and Y^{3+}-substitutional Li$^+$ ions in the Y$_2$O$_3$ host lattice. The tridoping of Li$^+$ ions thereby can result in a larger ion concentration of luminescent effective Yb^{3+} and Er^{3+} by increasing the optically active lattice sites (with a factor of 4/3 for each) in tailored Y$_2$O$_3$ nanocrystals. Consequently, the parameters that can lead to changed green UC intensities will be N_0, N_{Yb0}, β_{green}, and $\tau_{Yb}^2\tau_2$, which agrees well with the fact that the local crystal field is expected to be tailored by Li$^+$ ions. Additionally, the coefficient $(1/\beta_{green} - 1)$ in eq 5 can theoretically illustrate the ion dissociation effect that was induced by the Li$^+$ ions via hindering the CR and the EBT processes involved in the red UC generation (see Figure 7). This coefficient can lead to different enhancement times for the green and red UC luminescence.

3. Mechanisms for UC Enhancement. Figure 8 displays the decay profiles of the $^2F_{5/2}$ (Yb) → $^2F_{7/2}$ (Yb) transition at 1075 nm in Y$_2$O$_3$ nanocrystals tridoped with 0−15 mol % of Li$^+$ ions. The inset presents the contrasted NIR spectra in Y$_2$O$_3$ nanocrystals doped with 1 mol % of Er^{3+} and Y$_2$O$_3$ nanocrystals further doped with 2 mol % of Yb^{3+} ions under laser excitation of 970 nm, which agrees well with previous data.[3] It is worthwhile to point out that the decay profiles of the $^4I_{11/2}$ (Er) and $^2F_{5/2}$ (Yb) states at 1015 and 1075 nm, respectively, are almost the same (see Supporting Information), which may arise from their strong coupling.[30] Therefore, we obtain from eq 4 that

$$I_{green} = A\beta_{green}\tau_{Yb}{}^3(\sigma_{Yb}N_{Yb0}^{con})^2\rho^2(W_2W_0N_0^{con}) \quad (6)$$

$$\text{Enhancement} = A\beta_{green}(Li)\tau_{Yb}{}^3(Li)/[\beta_{green}(0)\tau_{Yb}{}^3(0)] \quad (7)$$

where A is a constant amplification factor that equals about 2.37 for all Li^+ ion doped nanocrystals due to the increased optical-active lattice sites (by a factor of 4/3) and equals 1 for Y_2O_3 nanocrytals without Li^+ ions, respectively. It is worthwhile to point out that the different symbols N_{Yb0}^{con} and N_0^{con} used here for the ion concentrations (compare to eq 4) represent the constant concentrations of the Yb^{3+} and Er^{3+} ions in all the samples, which is also equal for Y_2O_3 nanocrytals without Li^+ ions. The increased effective concentrations of Yb^{3+} and Er^{3+} ions due to the increased optically active lattice sites have been considered in the parameter A. It should be noted that the parameter β_{green}(Li) as function of Li^+ ions can be calculated according to eq 5 via the use of the intensity ratio of green to red UC in Figure 5. The parameter τ_{Yb}(Li) as a function of Li^+ ions can be experimentally measured according to Figure 8. Hence, the enhancement times for the green and red UC can easily be calculated according to eqs 7 and 5. The values of these parameters together with the calculated and observed enhancement times for the green and red UC radiations are compiled in Table 1.

As shown in Table 1, much larger lifetimes in the $^2F_{5/2}$ (Yb) and $^4I_{11/2}$ (Er) states were experimentally observed for Y_2O_3 nanocrytals tridoped with Li^+ ions. Such an observation seems to disagree with the results in Section 1 of the Discussion, because the nonradiative rates in the two states have not been changed by the Li^+ ions. Let us exemplify with the experimental lifetime in the $^2F_{5/2}$ (Yb) state, defined as follows;

$$1/\tau_{Yb} = 1/\tau_{Yb}^{rad} + W_{Yb}^{non} + W_{Yb}^{ET} \quad (8)$$

where τ_{Yb} is the experimentally measured lifetime, τ_{Yb}^{rad} is the calculated (or theoretical) lifetime, W_{Yb}^{non} is the nonradiative rate of the $^4I_{11/2}$ (Er) state, and W_{Yb}^{ET} is the energy transfer rate from the Yb^{3+} to the Er^{3+} ions. It is noted that W_{Yb}^{ET} is almost identical for all the nanocrytals due to the same ratio (also concentration) of Yb^{3+} to Er^{3+} ions for all samples. Actually, this parameter was slightly decreased by a factor of 1.1 for all the Li^+ ions, as suggested from the enhancement time analysis (see below). This slight anomaly, however, only has a very little contribution to the large lifetime increase observed for all Li^+ ions. As discussed in Figure 6, the nonradiative rate W_{Yb}^{non} for the $^2F_{5/2}$ (Yb) state is also nearly constant for all Y_2O_3 nanocrytals due to unchanged phonon cutoff energy. Consequently, the much larger lifetimes observed in the intermediate $^4I_{11/2}$ (Er) and $^2F_{5/2}$ (Yb) states must arise from the change of their theoretical lifetimes, which can be well explained by the fact that Li^+ ions can tailor the local

crystal field of the Y_2O_3 host lattice, and therefore can modify the theoretical lifetimes of rare earth ions by slightly changing their wave functions. It is worthwhile to mention that similar results were also observed for the other energy levels of Er^{3+} ions, which further evidence the great influence of the Li^+ ions. Theoretical computation of these lifetimes by use of the Judd−Ofelt theory can deliver a final clarification to the approach, which guarantees our further work.

The calculated enhancement in Table 1 for both the green and red UC display a large (15 times) and slight (only 1.6 times) fluorescence increase for Li^+ ion concentrations of 0−2 and 2−5 mol %, respectively, and a nearly constant enhancement at higher Li^+ ions. Such a tendency is in good agreement with the experimental observations in Figure 5, which suggest the correctness of the proposed enhancement mechanism. As illustrated in Table 1, the most important enhancement factors are the lifetime parameters in the intermediate $^4I_{11/2}$ (Er) and $^2F_{5/2}$ (Yb) states, which are tailored by the modified local crystal field via Li^+ ion doping. Such a phenomenon illustrates that tailoring the local crystal field of host materials (no matter what they are) via use of nonluminescent ions, for example, Li^+ ions, can become a general route for increasing of UC radiations in rare-earth ions. Quantitatively, the calculated enhancement times for both the green and red UC are slightly larger than the observed ones. Particularly, the enhancement values for Li^+ ion concentrations higher than 7 mol % are beyond the scope of the experimental error. To find out the reason for this, it is noted that the parameters W_0 and W_2 have been assumed to be constant in deriving eq 7, since the same ion concentrations of 2 mol % of Yb^{3+} and 1 mol % of Er^{3+} ions were utilized for all the samples. This expectedly leads to the same ion distance between the Er^{3+} and Yb^{3+} ions. However, the increased intensity ratio of the green to red UC illustrates that the Li^+ ions can greatly dissociate the Er^{3+} and Yb^{3+} clusters in the Y_2O_3 host lattice (see the Discussion about Figure 5), which in fact can lead to an increased effective average distance between Yb^{3+} and Er^{3+} ions. A larger distance will result in smaller ET coefficients W_0 and W_2, because they have a six power inverse dependence on the ion distance.[1] As shown in Table 1, the bracketed enhancement times were calculated by considering a slight decrease in the two parameters with a supposed reduction factor of 1.1, which corresponds to a reasonable increase of 1% in the effective average ion distance. As can be seen, all the calculated enhancement times agree well with the experimental ones.

An additional short comment regarding the overall UC fluorescent intensity in Li^+-ion-tailored Y_2O_3 nanocrytals is given below. As illustrated in eq 6, the high green fluorescence achieved benefits from (1) the multiplication of the much larger

TABLE 1: Measured Lifetimes (τ_{Yb}) of the $^2F_{5/2}$ (Yb) State, Calculated Parameter β_{green}, Constant Amplified Factor (A) Due to the Increased Optically Active Lattice Sites, Calculated and Experimental Enhancements for the Green and Red UC Radiations in Y_2O_3 Nanocrytals Doped with 1 mol % of Er^{3+} and 2 mol % of Yb^{3+} Ions and Further Tridoped with Various Li^+ Ion Concentrations[a]

					green enhancement (times)		red enhancement (times)	
Li^+ (mol %)	τ_{Yb} (ms)	$\tau_{Yb}{}^3$ (ms^3)	β_{green}	A	calculated	experiment (error 20%)	calculated	experiment (error 20%)
0	0.8 (2)	0.51	0.5	1	1	1	1	1
2	1.4 (1)	2.7	0.72	2.4	18 (15)	15	7.3 (6.0)	5.9
5	1.6 (1)	4.1	0.76	2.4	29 (24)	25	9.2 (6.8)	8.1
7	1.6 (1)	4.1	0.75	2.4	28 (23)	20	9.3 (7.7)	6.7
10	1.6 (1)	4.1	0.74	2.4	28 (23)	22	9.3 (7.7)	7.5
15	1.6 (1)	4.1	0.74	2.4	28 (23)	21	9.3 (7.7)	7.1

[a] The enhancement times in the brackets were calculated by considering the reduction of the ET coefficients between Yb^{3+} and Er^{3+} ions via a factor of 1.1.

absorption cross section (5 times larger than for Er^{3+} ions) and the Yb^{3+} ion concentration $(\sigma_{Yb}N_{Yb0})^2$ and (2) the tailoring effect induced by the Li^+ ions $A\beta_{green}\tau_{Yb}^3$, which includes the tailored radiation parameters, the increased optical-active lattice sites, and the ion cluster dissociations. These separated two parts interpret well the fact that the Yb^{3+} ion sensitization and the tailoring-effect induced by the Li^+ ions are two independent enhancement mechanisms for the UC radiations. Such conclusions have been initially demonstrated in our previous work and unpublished data via the use of Li^+ ions for significant UC enhancement in Er^{3+}-doped Y_2O_3 nanocrytals without Yb^{3+} ion doping and codoped with 10 mol % of Yb^{3+} ions, respectively. We believe that the simultaneous use of both enhancement mechanisms to increase the UC radiations in future works can greatly promote a number of photonic and biomedical applications.

Conclusions

Visible green and red UC emissions in $Y_2O_3/Yb^{3+}/Er^{3+}$ nanocrystals were enhanced by up to half of the bulk counterpart by tridoping with Li^+ ions, which can be contrasted to the usually 2 orders of magnitude higher UC radiations of the bulk compared to Li^+-free nanocrystals. XRD investigations illustrate that the local crystal field of the Y_2O_3 host lattice can be expectedly tailored by substituting the Y^{3+} ions or occupying the interstitial lattice sites with Li^+ ions. Decay time analysis evidenced that the observed much larger lifetimes in the Yb^{3+} and Er^{3+} ions arise from such tailoring induced by Li^+ ions. Theoretical calculations can well explain the observed significantly enhanced lifetimes, which arise from a synthesized tailoring effect—induced by Li^+ ions—of the lifetimes in the intermediate $^4I_{11/2}$ (Er) and $^2F_{5/2}$ (Yb) states, increased optically active lattice sites in the Y_2O_3 host lattice, and dissociation of the Yb^{3+} and Er^{3+} ion clusters in the nanocrytals. General theoretical descriptions of the visible UC radiations illustrate that the Yb^{3+} ion sensitization and the tailoring effect induced by Li^+ ions are two independent mechanisms for the UC radiation enhancement. The simultaneous use of the two enhancement mechanisms can expedite a number of photonic and biomedical applications in future, since both are expected to be independent of the host materials. Additionally, a remarkable enhancement of 3 times in ceramic bulk Y_2O_3 suggests the effectiveness of the Li^+ ions for bulk materials, which, however, requires an appropriate technique to dope large concentrations of Li^+ ion into the host lattice for higher enhancement times.

References and Notes

(1) Auzel, F. *Chem. Rev.* **2004**, *104*, 139.

(2) Suyver, J. F.; Aebischer, A.; Biner, D.; Gerner, P.; Grimm, J.; Heer, S.; Krämer, K. W.; Reinhard, C.; Güdel, H. U. *Opt. Mater.* **2005**, *27*, 1111.

(3) Vetrone, F.; Boyer, J. C.; Capobianco, J. A.; Speghini, A.; Bettinelli, M. *J. Phys. Chem. B* **2003**, *107*, 1107.

(4) Hinkliin, T. R.; Rand, S. C.; Laine, R. M. *Adv. Mater.* **2008**, *20*, 1270.

(5) Wang, X.; Kong, X. G.; Yu, Y.; Sun, Y. J.; Zhang, H. *J. Phys. Chem. C* **2007**, *111*, 15119.

(6) Zhang, J.; Wang, S. W.; An, L. Q.; Liu, M.; Chen, L. D. *J. Lumin.* **2006**, *8*, 122–123.

(7) Lim, S. F.; Riehn, R.; Ryu, W. S.; Khanarian, N.; Tung, C. K.; Tank, D.; Austin, R. H. *Nano. Lett.* **2006**, *6*, 169.

(8) Chen, G. Y.; Zhang, Y. G.; Somesfalean, G.; Zhang, Z. G.; Sun, Q.; Wang, F. P. *Appl. Phys. Lett.* **2006**, *89*, 163105.

(9) Wang, L. Y.; Li, Y. D. *Chem. Commun.* **2006**, 2557.

(10) Zhang, P.; Steelant, W.; Kumar, M.; Scholfield, M. *J. Am. Chem. Soc.* **2007**, *129*, 4526.

(11) Sivakumar, S.; M van, Veggel.; F. C., J.; Stanley May, P. *J. Am. Chem. Soc.* **2007**, *129*, 620.

(12) Matsuura, D. *Appl. Phys. Lett.* **2002**, *81*, 4526.

(13) Song, H. W.; Sun, B. J.; Wang, T.; Lu, S. Z.; Yang, L. M.; Chen, B. J.; Wang, X. J.; and Kong, X. G. *Solid State Commun.* **2004**, *132*, 409.

(14) Pires, A. M.; Serra, O. A.; Heer, S.; Güdel, H. U. *J. Appl. Phys.* **2005**, *98*, 063529.

(15) Vetrone, F.; Boyer, J. C.; Capobianco, J. A.; Speghini, A.; Bettinelli, M. *J. Appl. Phys.* **2004**, *96*, 661.

(16) Bai, X.; Song, H. W.; Pan, G. H.; Lei, Y. Q.; Wang, T.; Ren, X. G.; Lu, S. Z.; Dong, B.; Dai, Q. L.; Fan, L. B. *J. Phys. Chem. C* **2007**, *111*, 13611.

(17) Pires, A. M.; Serra, O. A.; Davolos, M. R. *J. Lumin.* **2005**, *113*, 174.

(18) Santos, P. V.; Gouveia, E. A.; Araujo, M. T.; Gouveia-Neto, A. S. *Appl. Phys. Lett.* **1999**, *74*, 3607.

(19) Gouveia-Neto, A. S.; Costa, E. B.; Bueno, L. A.; Ribeiro, S. J. L. *J. Alloy. Compd.* **2004**, *375*, 224.

(20) Yi, G. S.; Chow, G. M. *Chem. Mater.* **2007**, *19*, 341.

(21) Lü, Q.; Guo, F. Y.; Sun, L.; Li, A. H.; Zhao, L. C. *J. Phys. Chem. C* **2008**, *112*, 2836.

(22) Chen, G. Y.; Liu, H. C.; Somesfalean, G.; Sheng, Y. Q.; Liang, H. J.; Zhang, Z. G.; Sun, Q.; Wang, F. P. *Appl. Phys. Lett.* **2008**, *92*, 113114.

(23) Bai, Y. F.; Yang, K.; Wang, Y. X.; Zhang, X. R.; Song, Y. L. *Opt. Commun.* **2008**, *281*, 2930.

(24) Weber, M. J. *Phys. Rev.* **1968**, *171*, 283.

(25) Chen, G. Y.; Somesfalean, G.; Liu, Y.; Zhang, Z. G.; Sun, Q.; Wang, F. P. *Phys. Rev. B.* **2007**, *75*, 195204.

(26) Heer, S.; Kömpe, K.; Güdel, H. U.; Haase, M. *Adv. Mater.* **2004**, *16*, 2102.

(27) Guo, H.; Dong, N.; Yin, M.; Zhang, W. P.; Lou, L.; Xia, S. D. *J. Phys. Chem. B* **2004**, *108*, 19205.

(28) Capobianco, J. A.; Vetrone, F.; Boyer, J. C.; Speghini, A.; Bettinelli, M. *J. Phys. Chem. B* **2002**, *106*, 1181.

(29) Suyver, J. F.; Aebischer, A.; García-Revilla, S.; Gerner, P.; Güdel, H. U. *Phys. Rev. B* **2005**, *71*, 125123.

(30) Page, R. H.; Schaffers, K. I.; Waide, P. A.; Tassano, J. B.; Payne, S. A.; Krupke, W. F. *J. Opt. Soc. Am. B* **1998**, *15*, 996.